sustainability

MDPI

Article

Influence of Basalt Fiber on Mechanical Properties and Microstructure of Rubber Concrete

Xiao Wang [1,2,3], Jinggan Shao [2,4,*], Junchao Wang [2], Minghao Ma [3] and Bing Zhang [1]

1 School of Materials Science and Engineering, Zhengzhou University, Zhengzhou 450001, China
2 Green High-Performance Material Application Technology Transportation Industry Research and Development Center, Henan Jiaoyuan Engineering Technology Group Co., Ltd., Zhengzhou 451450, China
3 School of Materials Science and Engineering, North China University of Water Resources and Electric Power, Zhengzhou 450045, China
4 Henan College of Transportation, Zhengzhou 451450, China
* Correspondence: sjgjygs@163.com

Abstract: The utilization of waste rubber in concrete will reduce pollution and improve the efficiency of resource utilization. The effects of rubber particles and basalt fibers on the compressive strength and splitting tensile strength of concrete were investigated. In addition, the influence of basalt fibers on the mechanical properties and micropore structure of rubber concrete (RC) were analyzed using scanning electron microscopy (SEM) and X-ray computed tomography (CT). The distribution of rubber particles in concrete was also studied. The results indicate that the effects of basalts fibers on the mechanical properties of rubber concrete were significant. The rubber particles were evenly distributed in the concrete. Compared with normal concrete (NC), rubber concrete with 10% rubber particles had lower compressive strength and splitting tensile strength. Compared with rubber concrete, basalt fiber rubber concrete (BFRC) with 2% basalt fibers had no obvious effect on the compressive strength, while significantly improving the splitting tensile strength, refining the pores of rubber concrete, and reducing the porosity of the matrix. The effects of basalt fiber on the properties and pore distribution of RC should be considered in future applications.

Keywords: basalt fiber rubber concrete; CT; mechanical properties; pore structure; SEM

Citation: Wang, X.; Shao, J.; Wang, J.; Ma, M.; Zhang, B. Influence of Basalt Fiber on Mechanical Properties and Microstructure of Rubber Concrete. *Sustainability* **2022**, *14*, 12517. https://doi.org/10.3390/su141912517

Academic Editor: Jonathan Oti

Received: 8 August 2022
Accepted: 27 September 2022
Published: 30 September 2022

1. Introduction

Concrete is the world's most-consumed manufactured material. Substantial research has been carried out to enhance the engineering properties, rheology, durability, and sustainability of various types of concrete [1]. At present, global waste tire generation considerably exceeds consumption; waste rubber tires are a cause of concern, as huge volumes are being discarded and buried, thus causing serious environmental pollution [2]. Scholars have processed waste rubber to make rubber particles or rubber powder, and mixed it into concrete as aggregate to make rubber concrete [3]. The addition of rubber particles introduces gas and pores into the concrete, changing its internal structure [4], and improving its frost resistance and impermeability. The incorporation of rubber particles into concrete is of great significance in the field of concrete durability and environmental protection. At the same time, as an organic polymer material, rubber has a layer of hydrophobic substances on its surface, which cannot be well combined with inorganic cement-based materials, thereby greatly weakening the mechanical properties of rubber concrete. Several scholars have conducted mechanical experiments on rubber concrete [5] and measured a decrease in performance compared to normal concrete [6]. Atahan [7] measured a 96% decrease in strength at 100% rubber admixture compared to normal concrete. Therefore, although rubber particles improve the durability of concrete, they greatly weaken the mechanical properties.

Some scholars have improved the strength of rubber concrete by incorporating fibers. Qiuhong Zhao [8], Jianyong Pang [9], and others mixed steel fiber with a mass fraction of 0–1.5% into rubber concrete to analyze its cyclic compressive performance. The results showed that the steel fiber-reinforced rubber concrete had better cyclic compressive performance, obvious ductile characteristics in failure, and higher ductility and toughness. En Zhang [10], Aijiu Chen [11], and others studied the effect of polypropylene fiber on the working and mechanical properties of rubber concrete. The results showed that the slump of rubber concrete decreased significantly with the increase in fiber, the compressive strength increased first and then decreased with the increase in fiber, and the splitting tensile strength and flexural strength increased with the increase in fiber. Jinyan Wang [12] studied the improvement of the strength of rubber concrete with different content of carbon fiber. The results showed that, when the content of carbon fiber was 0.2%, the effect of improving the splitting strength of rubber concrete was better. When the content was 0.4%, the flexural strength gain was the highest, increasing by 39.71%, but the compressive strength was not significantly improved.

All the above fibers have certain disadvantages due to their characteristics. In comparison, the excellent overall performance of basalt fibers becomes a better choice. Some scholars have blended basalt fibers into rubber concrete, improving the compressive strength and splitting tensile strength of concrete to some extent [13–16]. Chen Meng [17] conducted a study on the effect of different amounts of basalt fibers on the mechanical properties of rubber concrete, and the results showed that the fibers were haphazardly distributed in the concrete during the mixing process and formed a three-dimensional network structure with the matrix, which successfully inhibited the generation and expansion of cracks, and substantially improved the mechanical properties of concrete.

The strength and durability of cement-based materials are closely related to their compactness, while the compactness of cement-based materials is closely related to porosity and pore structure. Chenchen Yang [14] used the mercury injection method to study the influence of basalt fiber on the porosity of rubber concrete. The results show that the basalt fiber improved the porosity distribution and optimized the pore structure. Mercury intrusion porosimetry (MIP) is a common method to test the pore structure of porous materials. However, MIP needs to pressurize the sample to hundreds of MPa to detect the nano pore structure, which may lead to the destruction of the pore wall of cement-based materials and affect the test results. Moreover, the pore structure tested by MIP assumes that the pores of the sample are cylindrical, which is different from the real pore structure of cement-based materials. Scanning concrete using CT [18] allows scanned images of the concrete interior, which, combined with the corresponding reconstruction software, allows visual analysis of the internal microstructure of concrete [19]. The use of the CT scan reconstruction method for pore analysis allows not only connectivity analysis but also characterization of the pores to a more accurate pore model [20].

The purpose of this paper is to use basalt fibers to reinforce rubberized concrete. First, the effects of rubber particles and basalt fibers on the mechanical properties of concrete were analyzed using compressive strength and splitting tensile strength as evaluation indicators. Then, the influence of the incorporation of rubber particles and basalt fibers on the concrete pore structure was studied using CT scanning technology and the reconstruction of the concrete pore structure model. Lastly, the effects of rubber particles and basalt fibers on the microstructure of concrete were analyzed using scanning electron microscopy.

2. Experimental Program

2.1. Performance Parameters of Raw Materials

The cement employed for the concrete material was ordinary Portland cement P.O.42.5, The chemical composition of cement is shown in Table 1. The coarse aggregate utilized natural stone with particle size ranging from 5 mm to 20 mm, with the apparent density of 2780 kg/m^3. The fine aggregate was natural river sand, with a fineness module of 1.91. Water was from the local tap without any additives, with a water–cement ratio of 0.36.

Superplasticizer was from Jiangsu Zhaogia Building Materials Technology Company, at the amount of 0.1% of the mass of cement. Rubber particles were from Henan Xuchang Chengli Recycling Resources Company, with a particle size less than 0.85 mm; the physical properties of rubber particles are shown in Table 2. Basalt fiber was from the Henan Dengdian Basalt Fiber Products Company, with an apparent density of 2610 kg/m^3; the performance parameters of basalt fiber are shown in Table 3.

Table 1. Chemical composition of cement (wt.%).

Chemical Composition	CaO	SiO_2	Al_2O_3	Fe_2O_3	MgO	SO_3	Others
Cement	61.74	16.44	4.78	3.52	2.67	3.69	7.16

Table 2. Rubber particle performance parameters.

Particle Size (mm)	Apparent Density (g/cm^3)	Bulk Density (g/cm^3)	Water Content (%)	Ash Content (%)
0.85	1.5	0.331	1.8	5.7

Table 3. Performance parameters of basalt fiber.

Density (g/cm^3)	Breaking Load (N)	Tensile Strength (MPa)	Elastic Modulus (GPa)	Breaking Elongation (%)
2.61	44.38	416.8	850	1.50

2.2. Concrete Mix Design and Molding

In the early stage of the experiment, the mixing ratio of concrete strength grade C50 was designed as OC, and, on this basis, the rubber particles with the volume content of 10% and 20% and the basalt fibers with the mass content of 0.1%, 0.2%, and 0.3% were designed in the orthogonal experiment. The results show that with the increase in the mass content of basalt fibers, the compressive strength of the matrix decreased and the splitting tensile strength increased; with the increase in the volume content of rubber particles, the compressive strength and flexural strength of the matrix decreased. On the premise of ensuring the strength of the matrix, the RC group with the volume content of rubber particles of 10% was selected, and the BFRC group with the volume content of rubber particles of 10% and the mass content of basalt fibers of 0.1% was selected.

The concrete mixing ratio is presented in Table 4. The test was designed according to the code for the standard design of mix proportion of ordinary concrete in China (JGJ 55-2011), eight 100 mm × 100 mm × 100 mm test blocks were formed in three groups: three for testing compressive strength, three for testing splitting tensile strength, and two for CT scanning.

Table 4. Concrete mixture proportions per 1 m^3.

Sample Types	Cement (kg)	Fine Aggregate (kg)	Coarse Aggregate (kg)	Water (kg)	Rubber Particles (kg)	Basalt Fiber (kg)	Superplasticizer (g)
OC	513.08	661.54	1074.47	185.00	0	0	685.77
RC	513.08	624.15	1074.47	185.00	21.41	0	685.77
BFRC	513.08	624.15	1074.47	185.00	21.41	2.6	685.77

In the process of casting, firstly, the cement, fine aggregate, rubber particles, basalt fiber, and coarse aggregate were weighed. The fine aggregate, coarse aggregate, basalt fiber, and rubber particles were introduced into the concrete mixer for 30 s of dry mixing, before adding cement and superplasticizer to continue dry mixing for 45 s. Finally, water was added for 150 s. the concrete was placed into a mold with dimensions of 100 mm × 100 mm × 100 mm to a level higher than the surface of the mold. Then, the vibrating table was initiated until the surface concrete came out of the slurry for smoothing treatment. When the smoothing was completed, the surface of the test block was covered with a layer of cling film. After curing for 24 h, all molds are demolded, and the specimens were cured in a standard curing room within the temperature range of 20 ± 3 °C and a humidity in excess of 95% for 28 days. The rubber particles and basalt fiber used during the casting are shown in Figure 1.

(**a**) (**b**)

Figure 1. Rubber particles and basalt fibers: (**a**) rubber particles; (**b**) basalt fibers.

2.3. Test Methods of Mechanical Properties

Mechanical properties of hardened concrete were tested according to China Standards GB/T50081-2019 after curing for 28 days. A four-column servo-hydraulic machine was used for the compressive test. Before the experiment, the surface of the test block and the bearing plate of the test machine were wiped clean; then, the side perpendicular to the molding surface was selected as the pressed surface, and the test block was placed in the center of the bearing surface. The tester was started, and continuous loading was ensured during the test.

According to the requirements of the standard test method of mechanical properties on ordinary concrete GB/T50081-2019, the formulae for calculating compressive strength and tensile strength are shown in Equations (1) and (2).

$$f_{CC} = \frac{F}{A}, \tag{1}$$

where f_{cc} is the cubic compressive strength of the concrete specimen (MPa), F is the magnitude of the load when the specimen is damaged by compression (N), and A is the area of the specimen subjected to the load (mm^2).

$$f_{ts} = \frac{2F}{\pi A} = 0.637\frac{F}{A}, \tag{2}$$

where f_{ts} is the tensile strength of the concrete specimen (MPa), F is the magnitude of the load when the specimen is damaged by compression (N), and A is the area of the specimen subjected to the load (mm^2).

In addition, since nonstandard specimens were used, the final strength was multiplied by the corresponding dimensional coefficient of 0.95.

2.4. Microstructure Analysis

As the CT scanning equipment requires a cylindrical shape of the specimen, the concrete specimen was cored using a drilling and sampling machine. When coring, the forming surface of the specimen was placed above, and the core was taken from center of the specimen, with a size of 50 mm in diameter and 100 mm in height, as shown in Figure 2.

Figure 2. CT scan specimen.

The CT scanning equipment was a Phoenix V∣tome∣xs series industrial X-ray CT scanner, manufactured by GE, Germany, with a scanning resolution of about 18 μm. A total of 1700 slices with a spacing of about 58.86 μm were obtained from this scan. Models of slice data obtained from CT scans were generated using Avizo software.

Before the SEM test, gold spraying was performed. The samples were subjected to a Quanta 250 FEG field-emission scanning electron microscope under the conditions of 5 kV accelerating voltage to observe the microscopic morphology and the presence of rubber particles and basalt fiber in concrete.

3. Experimental Results

3.1. Concrete Failure Mode

In the process of the compressive test, cracks were produced around the OC specimen, and the cracks expanded rapidly with the gradual increase in the load; when the load reached the ultimate concrete load, a violent sound was issued, and a large area around the edge fell off, showing obvious brittle failure, as shown in Figure 3a. RC produced some small cracks on the surface in the process of compression, which expanded rapidly to all sides with the increasing load and became gradually obvious. Then, the particles fell off around the specimen, and, when the ultimate load is reached, there was no obvious sound, whereby the rubber admixture buffered part of the stress when the specimen was compressed, and the damage form of the specimen was also much more complete compared with plain concrete, as shown in Figure 3b. BFRC did not have any obvious changes at the beginning of the test process, until after reaching the ultimate load, when the cracks rapidly expanded and fell off around the specimen, showing obvious ductility, as shown in Figure 3c.

(**a**) (**b**) (**c**)

Figure 3. The compressive test of concrete (**a**) Ordinary concrete; (**b**) rubber concrete; (**c**) basalt fiber rubber concrete.

In the process of the splitting tensile test, obvious cracks appeared when the OC specimens were subjected to the load, and the cracks expanded rapidly with the gradual increase in the load. When the load reached the ultimate concrete load, a large sound was made and the specimen fractured, with small pieces falling off, as shown in Figure 4a. The process of RC produced some vertical cracks on the surface, which expanded rapidly along the vertical direction with increasing load and became gradually obvious. When the ultimate load was reached, the same obvious sound was made, but the test block was split into two intact halves, where it can be seen that the addition of rubber improved the toughness of the concrete, as shown in Figure 4b. BFRC was roughly the same as RC when loaded, but it did not make obvious sound when the ultimate load was reached, and the direction of crack expansion showed a curved shape, whereby the fibers in the concrete played a role in preventing the expansion of cracks, and the concrete test block that was not split into two halves. When trying to separate the test block by hand, the fibers in the test block still played a role, and the whole destruction process showed a certain ductility, as shown in Figure 4c.

(**a**) (**b**) (**c**)

Figure 4. The splitting tensile test of concrete (**a**) Ordinary concrete; (**b**) rubber concrete; (**c**) basalt fiber rubber concrete.

3.2. Strength Analysis

The data of compressive strength and splitting tensile strength are shown in Tables 5 and 6. According to the results of the compressive strength of concrete specimens (Figure 5), the admixture of rubber particles decreased the strength of concrete by 19.36%, while, after adding basalt fiber, the compressive strength was slightly improved, but still did not reach the level of plain concrete. After the RC was incorporated into the concrete, due to the very low strength of rubber particles, the deformation of the force area was reduced when subjected to load, which inevitably made the compressive strength of concrete lower than that of plain concrete. After the incorporation of basalt fiber, it was distributed in the concrete matrix during the process of mixing, and it bore part of the deformation when the concrete received the load, which slowed the generation and expansion of cracks inside the concrete. However, with the gradual increase in load, new cracks were inevitably generated and damage eventually occurred. The fibers slowed the destruction of the test block when the load gradually increased; therefore, the damaged test block still maintained a more complete shape.

Table 5. Compressive strength of the three concrete specimens.

Sample Types	Data 1 (MPa)	Data 2 (MPa)	Data 3 (MPa)	Average Splitting Tensile Strength (MPa)	Standard Deviation
OC	67.71	68.24	68.86	68.27	0.576
RC	54.12	54.28	56.75	55.05	1.474
BFRC	55.72	56.48	56.4	56.20	0.417

Table 6. Splitting tensile strength of the three concrete specimens.

Sample Types	Data 1 (MPa)	Data 2 (MPa)	Data 3 (MPa)	Average Splitting Tensile Strength (MPa)	Standard Deviation
OC	3.98	4.12	3.93	4.01	0.098
RC	2.75	3.12	2.74	2.87	0.216
BFRC	3.28	3.65	3.24	3.39	0.226

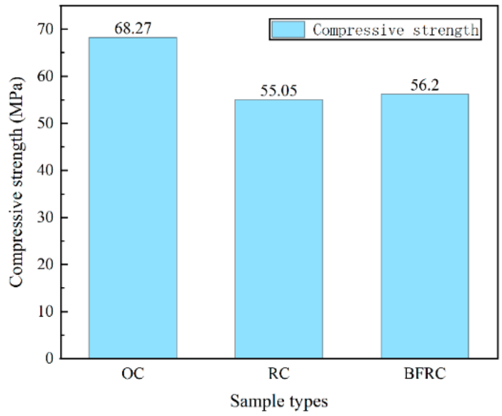

Figure 5. Compressive strength of the three concrete specimens.

The results of the splitting tensile strength of concrete specimens (Figure 6) show that the admixture of rubber particles decreased the strength of concrete by 28.43%, while the splitting tensile strength increased after the addition of basalt fibers, which exceeded the RC, but still had a certain difference compared to the plain concrete. As the rubber particles were small, elastic, and uniformly distributed inside the concrete, they effectively filled the internal pores of concrete; however, when subjected to external load, the macroscopic cracks were transformed into a large number of microscopic cracks, which reduced the splitting tensile strength of concrete. Basalt fibers were haphazardly distributed within the matrix after being incorporated into the concrete, and the fibers could be viewed as small reinforcement bars. Not only could they effectively inhibit the generation of cracks inside the concrete during the process of hydration and formation, but they could also assume part of the stress when subjected to external load, effectively slowing the stress concentration at the crack tip and inhibiting the further expansion of cracks during the loading process. Accordingly, the splitting tensile strength was increased by nearly 20% compared to RC.

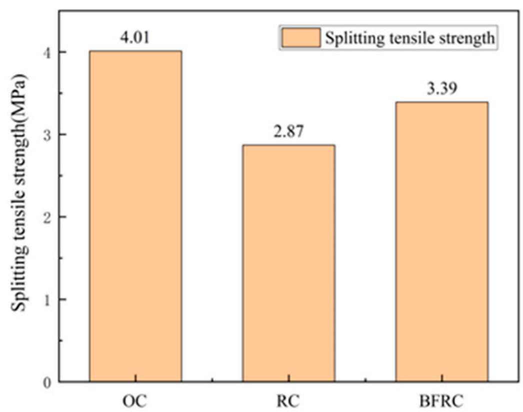

Figure 6. Splitting tensile strength of the three concrete specimens.

3.3. SEM Analysis

At the initial stage of load, the strain generated in the matrix was very small, and the tensile stress borne by the basalt fiber was relatively small. The concrete bore most of the tensile stress. With the increase in load, the strain generated in the matrix began to increase, and the tensile stress borne by the basalt fiber also increased (see Figure 7a). Adding basalt fiber into the rubber concrete delayed the generation of the initial crack of the specimen to some extent. After the concrete cracked, the stress between cracks was redistributed, and part of the pressure originally borne by the concrete was transferred to the basalt fiber. The fiber between the cracks transferred the load to the matrix on both sides (see Figure 7b), such that the concrete at the crack continued to bear the load, while the stress concentration between the cracks was alleviated. A stable stress field was still formed in the concrete, and crack propagation was effectively restrained. As more basalt was used to transfer the stress, the crack propagation time and the corresponding splitting tensile strength increased. The randomly distributed fibers (see Figure 7c) were staggered in the matrix in a grid-like structure, which could change the direction of crack extension or form a smaller crack field to restrict the crack expansion. However, a higher fiber content did not lead to more fibers blocking the crack formation. When the fibers were not evenly dispersed, they existed in bundles (see Figure 7d). Because of their water absorption, the water–cement ratio was large, and the strength of the generated cementitious material was low. When the matrix was stressed, the fibers could not bond well with the matrix and fall off, thus resulting in a pull-out fracture mark.

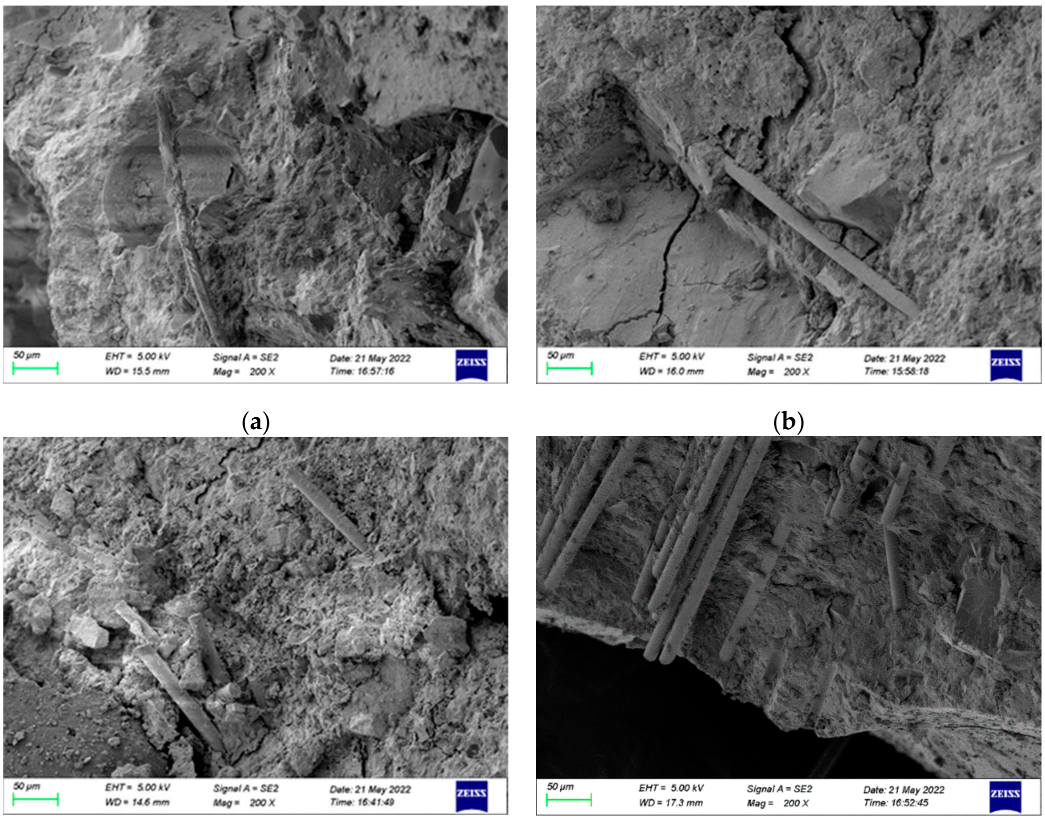

(**a**) (**b**)

(**c**) (**d**)

Figure 7. SEM images of basalt fiber in concrete: (**a**) Broken basalt fiber in concrete; (**b**) The basalt fiber between the cracks in concrete; (**c**) Basalt fibers disturbed in concrete; (**d**) Basalt fiber pull-out in concrete.

The pore models and data were obtained by processing the CT slice data using watershed segmentation and volume rendering in Avizo software. Figure 8 shows the internal pore structure models for the three types of concrete, allowing the distribution of the pores inside the concrete to be visualized. Figure 9 shows the number of pores and the number distribution of pores with different volumes.

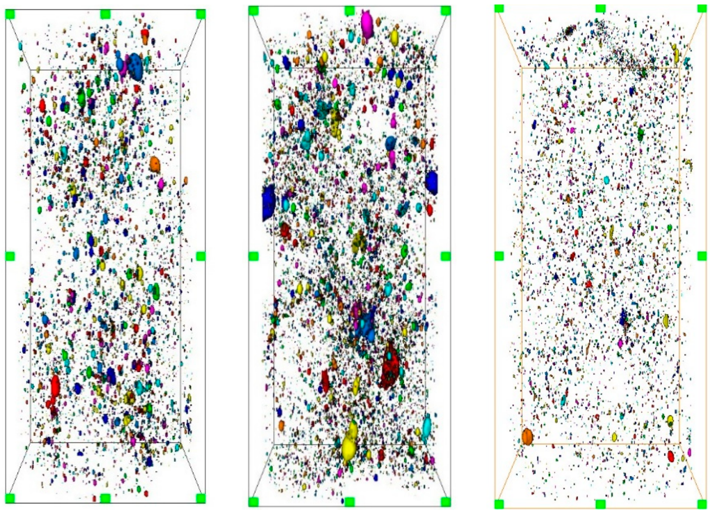

(**a**) (**b**) (**c**)

Figure 8. The 3D visualization model of concrete pore space: (**a**) ordinary concrete; (**b**) rubber concrete; (**c**) basalt fiber rubber concrete.

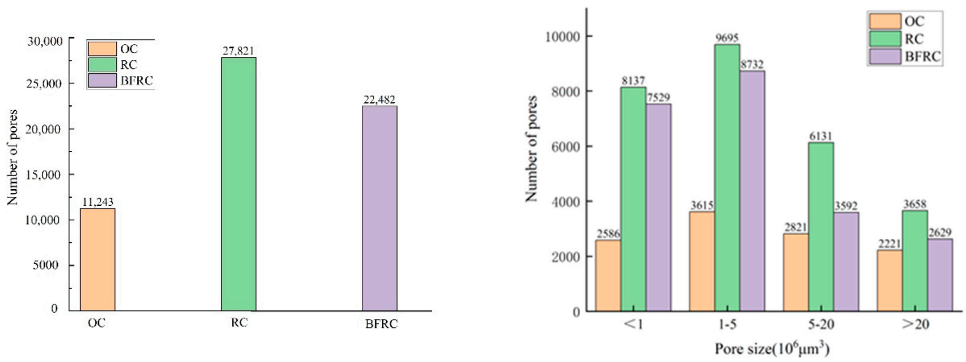

(**a**) (**b**)

Figure 9. Pore data: (**a**) total porosity volume; (**b**) pore size distribution.

According to Figure 8a, with the addition of rubber particles, the number of pores in concrete increased significantly; compared with the OC group, the RC group increased by 147.45%, because rubber is a high-molecular-weight organic substance and cement paste is an inorganic compound, which cannot be closely combined. Accordingly, the gas adsorbed by the rubber particles could not be effectively removed during concrete mixing, and the gas adsorbed by rubber particles could not be completely removed by subsequent mechanical vibration, resulting in an increase in the number of concrete pores.

When basalt fiber was added to the rubber concrete, the number of pores was greatly reduced, and the BFRC group was reduced by 19.19% compared with the OC group. Referring to Figure 8b, when the pore volume was less than 10^6 μm^3, the BFRC group reduced 608 holes compared with the RC group; when the pore volume was between 10^6 μm^3 and 5×10^6 μm^3, the BFRC group reduced 963 holes compared with the RC group; when the pore volume was between 5×10^6 μm^3 and 20×10^6 μm^3, the BFRC group reduced 2539 holes compared with the RC group; when the pore volume was greater than 20×10^6 μm^3, the BFRC group reduced 1029 holes compared with the RC group. This is because basalt fiber is an inorganic nonmetallic material with good compatibility with the cement matrix, and its fiber diameter was 14 μm. When the basalt fiber was mixed into the rubber concrete, the tiny fibers could fill the pores, showing good water absorption. The water adsorbed by the fiber reacted with the cement to form silicate gel. These cementitious materials filled the pores, refined the pore diameter, reduced the number of large pores, and increased the compactness of the matrix. Therefore, the number of concrete pores decreased.

According to Figure 10a, with the incorporation of rubber particles, the porosity of the RC group increased by 0.394% compared with the OC group. Combined with Figure 10b, the porosity of the RC group was large at the heights of 8 mm, 18 mm, 32 mm, and 52 mm, corresponding to the positions with large porosity in Figure 8b. This shows that rubber particles caused an uneven distribution of internal pores while increasing internal porosity. When basalt fiber was incorporated, the porosity of the BFRC group was reduced by 0.16% compared with the RC group, and the incorporation of basalt fiber reduced the number of pores; as shown in Figure 9b, the pores of the BFRC group were more evenly distributed than those of the RC group. This is because basalt fibers were evenly distributed after being mixed into the matrix and interlaced with each other, forming a grid skeleton, generating a certain binding force, and inhibiting the movement of rubber particles with small density during concrete vibration and molding.

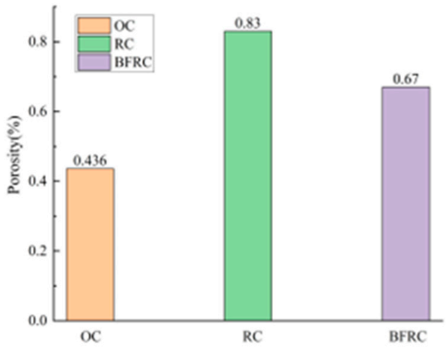

(**a**)

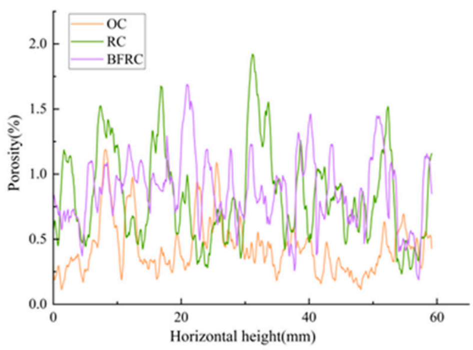

(**b**)

Figure 10. Porosity of concrete: (**a**) total porosity; (**b**) porosity distribution.

3.4. Distribution of Rubber Particles in Concrete

Rubber particle distribution maps of RC were obtained by processing CT slice data of rubber concrete using watershed segmentation and volume rendering in Avizo software. The points shown in Figure 11 are the rubber particles in the concrete. As can be seen from Figure 11, the rubber particles were evenly distributed in the concrete.

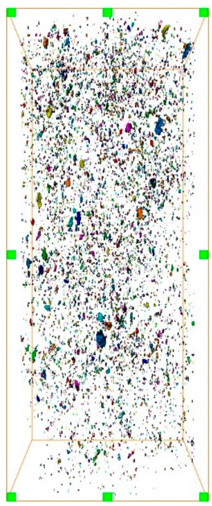

Figure 11. The 3D visualization model of rubber distribution in concrete.

4. Conclusions

In this paper, the effects of rubber particles and basalt fibers on the mechanical properties and pore distribution of concrete and their relationships were investigated using mechanical property experiments, CT scan modeling, and SEM image analysis based on ordinary concrete, and the following conclusions could be drawn:

(1) In the process of the compression test and splitting tensile test, the concrete of the OC group showed obvious characteristics of brittle failure, while the concrete of the RC group and BFRC group showed characteristics of ductile failure. Compared with the compressive strength and splitting tensile strength, the basalt fiber had no obvious effect on improving the compressive strength of rubber concrete. Its main role was to give play to the characteristics of tensile strength of fiber to improve the splitting tensile strength of rubber concrete.

(2) The addition of fiber could delay the generation of the initial crack of the test block. When the crack occurred, the stress between the fibers was redistributed, the fiber and the matrix were stressed at the same time, and the stress concentration between the cracks was alleviated, thus restraining crack propagation.

(3) The incorporation of rubber particles introduced a large number of pores, which were unevenly distributed. The incorporation of basalt fiber could refine the macropores and make the pore distribution more uniform. The rubber particles were evenly distributed in the concrete.

Author Contributions: Conceptualization, J.S. and X.W.; methodology, M.M.; software, X.W.; validation, X.W., M.M., and J.W.; formal analysis, X.W.; investigation, X.W.; resources, J.S.; data curation, X.W.; writing—original draft preparation, X.W.; writing—review and editing, X.W.; visualization, M.M.; supervision, J.S.; project administration, J.W. and B.Z.; funding acquisition, J.S. All authors have read and agreed to the published version of the manuscript.

Funding: This research was funded by Henan Provincial Department of Transportation Technology Project, grant number 2020J-2-11.

Institutional Review Board Statement: Not applicable.

Informed Consent Statement: Not applicable.

Data Availability Statement: Not applicable.

Conflicts of Interest: The authors declare no conflict of interest.

References

1. Mayhoub, O.A.; Abadel, A.A.; Alharbi, Y.R. Effect of Polymers on Behavior of Ultra-High-Strength Concrete. *Polymers* **2022**, *14*, 2585. [CrossRef] [PubMed]
2. Lamiaa, A.; Yasser, A. Properties of Rubberized Concrete Prepared from Different Cement Types. *Recycling* **2022**, *7*, 39.
3. Fedroff, D.; Ahmad, S. Mechanical Properties of Concrete with Ground Waste Tire Rubber. *Transp. Res. Rec.* **1996**, *1532*, 66–72. [CrossRef]
4. Qi, C.H. *Study on Mechanical Properties and Fracture Toughness of Porous Cement Concrete with Polymer Rubber Framework*; Chongqing Jiaotong University: Chongqing, China, 2020.
5. Xiong, J.; Zheng, L.; Yuan, Y. Experimental study on compressive strength of waste rubber concrete. *Concrete* **2004**, *12*, 40–42.
6. Yu, Z.; Tang, R.; Li, F. Experimental Study and Failure Criterion Analysis on Combined Compression-Shear Performance of Rubber Concrete (RC) with Different Rubber Replacement Ratio. *Constr. Build. Mater.* **2021**, *288*, 123105. [CrossRef]
7. Atahan, A.O.; Yücel, A.Ö. Crumb Rubber in Concrete: Static and Dynamic Evaluation. *Constr. Build. Mater.* **2012**, *36*, 617–622. [CrossRef]
8. Zhao, Q.; Dong, S.; Zhu, H.; Yu, Y. Stress strain relationship of steel fiber reinforced rubber concrete under cyclic compression. *J. Build. Mater.* **2022**, 1–13.
9. Pang, J.; Zhang, Q.; Yao, W.; Su, Q. Mechanical property test of steel fiber reinforced rubber concrete. *Chin. Sci. Technol. Pap.* **2020**, *15*, 1302–1307.
10. Zhang, E.; Lu, G.; Yang, H.; Zhao, Z. Experimental study on working and mechanical properties of polypropylene fiber reinforced rubber concrete. *Concrete* **2021**, 86–89.
11. Chen, A.; Chen, M.; Wang, D.; Hu, F.; Li, H. Experimental study on the basic properties of polypropylene fiber recycled rubber concrete. *Concrete* **2014**, 57–60.

12. Wang, J.; Wu, F.; Li, F. Experimental study on improving mechanical properties of rubber concrete with carbon fiber and micro silica fume. *China Water Transp.* **2021**, *21*, 158–160.
13. Han, K. *Properties and Mechanism of Multi-Scale Fiber Reinforced Cementitious Materials*; Harbin Institute of Technology: Harbin, China, 2017.
14. Yang, C.C.; Bai, Y. Study on the mechanical properties of rubber-doped powder and fiber concrete. *China Sci. Technol. Pap.* **2016**, *11*, 1548–1550.
15. Zhang, S.; Bai, Y. Mechanical properties tests and microscopic analysis of basalt fiber-doped rubber light-aggregate concrete. *World Concr.* **2020**, 66–69.
16. He, D.; Wang, J. Effect of rubber doping on physical and mechanical properties of CBFRC. *J. Constr. Mater.* **2015**, *18*, 857–860.
17. Chen, A.; Chen, M. Effect of basalt fibers on the mechanical properties of rubber recycled concrete. *Concrete* **2015**, 59–62.
18. Tan, Y. Computed tomography. *J. Bethune Med. Univ.* **1979**, 120–128.
19. Ruan, X.; Akiyama, M. Modelling Method of Fiber Distribution in Steel Fiber Reinforced Concrete Based on X-Ray Image Recognition. *Compos. Part B Eng.* **2021**, *223*, 109124.
20. Li, N. Research progress in studying internal damage of concrete based on X-ray CT technology. *Mater. Guide* **2021**, *35*, 21169–21177.